Materials Science in Semiconductor Processing 173 (2024) 108148

Contents lists available at ScienceDirect

Materials Science in Semiconductor Processing

journal homepage: www.elsevier.com/locate/mssp

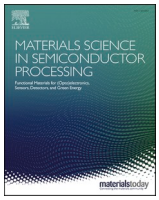

New method for the deposition of thin films on the inner walls of a deep blind hole: Application to semiconductor doping

Gianluigi Maggioni [a,b,*], Stefano Bertoldo [a,b], Chiara Carraro [b], Walter Raniero [b], Francesco Sgarbossa [a,b], Enrico Napolitani [a,b], Davide De Salvador [a,b]

[a] Dipartimento di Fisica e Astronomia, Università degli Studi di Padova, Via Marzolo 8, 35131, Padova, Italy
[b] INFN-Laboratori Nazionali di Legnaro, Viale dell'Università 2, 35020, Legnaro, Italy

ARTICLE INFO

Keywords:
Film deposition in a hole
High aspect ratio
High purity germanium
Pulsed laser doping
p+ doping
n+ doping

ABSTRACT

A novel method for the deposition of thin films of dopant elements on the inner walls of a hole with a high aspect ratio aimed at doping germanium is here described. $GeAl_x$ and Sb were evaporated from a W filament inserted inside a hole 10 mm in diameter and 80 mm deep (aspect ratio 8:1). The filament was previously coated by sputtering with either $GeAl_x$ or Sb film. The filament heating process is fast enough to ensure very limited temperature increase on the inside walls of the hole as demonstrated by a heat balance calculation, thus preventing the introduction of contaminant species in the doped semiconductor. The filament was inserted in a purpose-built sample holder where planar substrates acted as the inner walls of the hole. The thickness distribution of the films evaporated on these substrates was characterized and correlated with the thickness distribution of the sputtered films deposited on the filament. In view of the final application of this process, i.e., doping of coaxial Ge-based gamma radiation detectors, $GeAl_x$ and Sb films were evaporated on Ge substrates and then subjected to pulsed laser melting to induce metal diffusion and doping of Ge surface. Measurements of the electrical activation of the laser melted samples pointed out the successful doping by both elements, i.e., p + doping for Al and n + doping for Sb.

1. Introduction

The deposition of thin films on the inner walls of a deep blind hole (high aspect ratio) is a task of particular interest for many technological applications [1,2]. Most of the research in the last few years has focused on very small size holes and trenches (microns to tens of microns) for applications in micro-nanoelectronics including miniaturization and high-level integration of semiconductor devices [3–5]. However, larger holes with similar aspect ratios are also interesting and typically pose a technological challenge in the case of deposition processes, which by their nature are non-conformal, such as physical vapour deposition (PVD) techniques (e.g., evaporation and sputtering). As aspect ratios increase, sidewall coverage of physically-vapour-deposited films decreases dramatically.

One of the technological applications, in which the deposition of thin films on the internal walls of a deep hole is required, concerns the fabrication of complex, gamma radiation detectors [6]. These detectors are made of hyperpure germanium (HPGe) crystals of cylindrical shape, with a blind hole of diameter up to 10 mm and depth up to 80 mm (aspect ratio 8:1). The crystals work as diodes: the internal walls of the hole are the blocking contact (p + or n + contact) and the outer cylindrical surface is the rectifying contact (n + or p + contact, respectively). In commercially available detectors the p + contact is commonly produced with the boron ion implantation technique, which does not require post-implantation annealing treatments but uses a very expensive production plant. On the other hand, the n + contact is obtained with lithium evaporation and diffusion, which produces a very robust contact, but also very thick (up to 1 mm), not thermally stable and only roughly segmentable [7]. The use of alternative technologies to make contacts would be welcome to overcome the limits of current technologies, but is severely limited by the stringent properties of the detector, in particular the hyperpurity of germanium (impurity levels $\leq 1 \times 10^{10}$ atoms cm^{-3}), which must be preserved throughout the detector manufacturing process. This implies that high purity precursor materials are mandatory for making contacts and that Ge crystals must be kept at temperatures lower than 350-400 °C. These requirements preclude the

* Corresponding author. Dipartimento di Fisica e Astronomia, Università degli Studi di Padova, Via Marzolo 8, 35131, Padova, Italy.
E-mail address: gianluigi.maggioni@unipd.it (G. Maggioni).

https://doi.org/10.1016/j.mssp.2024.108148
Received 13 November 2023; Received in revised form 15 January 2024; Accepted 17 January 2024

use of conformal coating techniques such as chemical vapour deposition, which would be more suitable for deposition inside cavities, but which are characterized by too high process temperatures. For the same reason, dopant diffusion processes based on standard thermal treatments cannot be exploited either [8]. On the other hand, low-temperature techniques such as PVD and sputtering in standard configuration are not suitable because line-of-sight deposition would produce a film with very uneven thickness going from the entrance to the end of the hole. The monolayer doping technique [9] could be an interesting alternative for the deposition of doping species inside cavities, but it has some drawbacks related to the limited amount of doping atoms to be deposited and, in some cases, the too high deposition temperature [10,11]. In the future, exploring the use of precursors that have shown excellent results with planar geometries [12,13] is not ruled out, provided that the high purity of germanium is preserved.

In this work we will describe a relatively simple method for the deposition of a film containing a dopant element on the internal walls of a blind hole with a diameter of 10 mm and an aspect ratio up to 8:1. The method consists in the evaporation of a metal dopant from a tungsten filament. Two metal dopants are tested: Al (p + dopant) is co-evaporated with Ge while Sb (n + dopant) is evaporated alone. To the best knowledge of the authors, despite the wide application of metal-coated filaments for the vacuum evaporation and deposition of thin films [14], this method has not been used previously to coat the internal walls of a blind hole and to make contacts in a germanium detector. Luke [15] achieved the deposition of a 1-μm thick gold film on the inner walls of a hole in a coaxial detector using a very thin gold filament but the n + contact had previously been made by Li diffusion. Aluminum-coated tungsten filaments are routinely used for the production of UV mirrors [16] and for the deposition of metal electrodes on HPGe planar detectors [17]. Moreover, Cr-plated tungsten rods used for thin adhesion layers can be found on the market, but none of them are designed for depositions inside a blind hole.

The first step of the proposed method consists in the deposition by sputtering of either Al and Ge or Sb by sputtering on the tungsten filament. In order to characterize every single step of the method, the thickness of these dopant source layers is measured by Energy Dispersive X-ray Spectrometry (EDS) in different positions on the filament. As a next step the filament is inserted in a purpose-built sample holder where planar substrates act as the inner walls of the hole. The filament is then heated for a short time until the film evaporates. The thickness of $GeAl_x$ and Sb evaporated films is measured by Rutherford Backscattering Spectrometry (RBS) and correlated to the thickness of the source layers deposited on the filament. Taking into account the high temperature reached by the filament, the heating of the walls of the hole during evaporation is calculated to rule out an excessive increase of the temperature of the walls. In order to explore the application of this method to semiconductor doping, $GeAl_x$ and Sb films are also evaporated on Ge substrates and then subjected to pulsed laser melting (PLM) to promote the dopant diffusion inside the Ge matrix. Diffusion profiles of aluminum in the lasered samples are measured by Secondary Ion Mass Spectrometry (SIMS). Electrical Van der Pauw-Hall measurements of the lasered samples are used to study the activation of dopant atoms and the carrier concentration (holes for Al doping and electrons for Sb doping).

2. Experimental

2.1. Film deposition and treatment

The Ge, Al and Sb layers were deposited on W filaments (0.75 mm diameter) and different planar substrates by sputtering using an equipment consisting of a stainless-steel vacuum chamber evacuated by a turbomolecular pump at a base pressure lower than $1x10^{-4}$ Pa. Before sputtering deposition, the filaments were heated in vacuum in order to remove the volatile tungsten oxides present on the surface [14], which could contaminate the films deposited on the HPGe crystal and, after the laser process, the crystal itself. After this step the filaments were kept under inert atmosphere until sputtering deposition to limit the re-oxidation. The chamber was equipped with 2" cylindrical magnetron sputtering sources, connected to radio frequency power generators (Advanced Energy, 600 W, 13.56 MHz). The deposition parameters used for the films were: target-to-substrate distance 22 cm; working gas Ar (99.9999 % purity); Ar flow 100 sccm; working pressure around 0.75 Pa; direct RF power: 60 W (Ge), 60 W (Al) and 30 W (Sb). Pure Ge (99.999 %), Al (99.999 %) and Sb (99.999 %) were used as targets. The substrates used in the sputtering depositions were silicon wafers and carbon-coated silicon wafers for the measurements of the elemental doses carried out both by Rutherford Backscattering Spectrometry (RBS) and by Energy Dispersive Spectrometry (EDS) (see Results and discussion). The elemental doses (in atoms cm^{-2}) can be converted into equivalent physical thicknesses (e.g. in nm) by dividing them by the corresponding atomic densities (in atoms cm^{-3}). The tabulated atomic densities of the three elements studied in this work are: $6.023x10^{22}$ atoms cm^{-3} (Al), $4.429x10^{22}$ atoms cm^{-3} (Ge) and $3.273x10^{22}$ atoms cm^{-3} (Sb). The deposition rates were determined by RBS and the deposition runs were timed to achieve the desired film thickness.

In the case of aluminum, it has been shown that oxygen can inhibit the Al activation [18]. Oxygen incorporation in the Ge-Al films can occur in several steps of the process, i.e.: during the sputtering deposition, while the filament is in the air, during the evaporation and when the evaporated films are in the air before laser annealing. To reduce O incorporation, some precautions were adopted: first Al deposition rate during sputter deposition was kept significantly high to increase the ratio between the flow of Al atoms on the substrate and that of oxygen-containing gaseous species. Moreover, sputtering depositions were carried out in static mode: a first deposition was made on one side of the wires, holding the sample holder still, then a second deposition was carried out on the other side after having rotated the holder 180°. In this way the deposited atoms are continuously covered by other condensing atoms and their direct exposure time to the oxygen-containing residual species present in the chamber is shortened compared to a deposition in dynamic mode (i.e. with the sample holder continuously rotating). Even if the latter mode can assure a higher film homogeneity on the cylindrical surface of the wires, taking into account the very small wire diameter (0.75 mm), the deposition on surfaces not directly facing the target (in particular the shaded surface) is not negligible and can partially smooth out the film inhomogeneity. Another precaution concerned the sequence of deposition of aluminum and germanium: Al and Ge were not co-deposited, but a bilayer structure was adopted, with an Al film coated by a Ge film (cap layer), to hinder the interaction between Al and the oxygen-containing gaseous species present in the air. Finally, base pressure in the evaporation chamber was kept as low as possible (pressure $< 2x10^{-5}$ Pa).

The experimental equipment used for the Ge, Al and Sb evaporation from the W filament is comprised of a stainless-steel vacuum chamber evacuated by a turbomolecular pump. The filament coated by the sputtered film was inserted in a purpose-built dummy (substrate holder) with an 8 cm deep and 1 cm wide (diameter) hole (Fig. 1). The holder, which mimics a HPGe coaxial crystal, can accommodate two rows of 4 mm wide substrates along its entire length and one substrate on the floor of the hole facing the filament tip. The films were evaporated on different substrates: C-coated silicon wafers for measurement of Ge, Al and Sb doses by RBS and germanium wafers (electrical resistivity of 50 Ωcm) for electrical activation measurements. The voltage on the filament was measured by a digital multimeter and the current by an amperometric clamp (10 mA resolution).

The diffusion of the dopant layer into the Ge matrix was obtained through Pulsed Laser Melting (PLM), using an excimer KrF laser (Coherent COMPex 201F), emitting light at $\lambda = 248$ nm, with 22 ns pulse duration, over a square spot 5×5 mm^2 with 2 % uniformity, at 1 Hz repetition rate. Energy densities up to 500 mJ cm^{-2} were used for the samples.

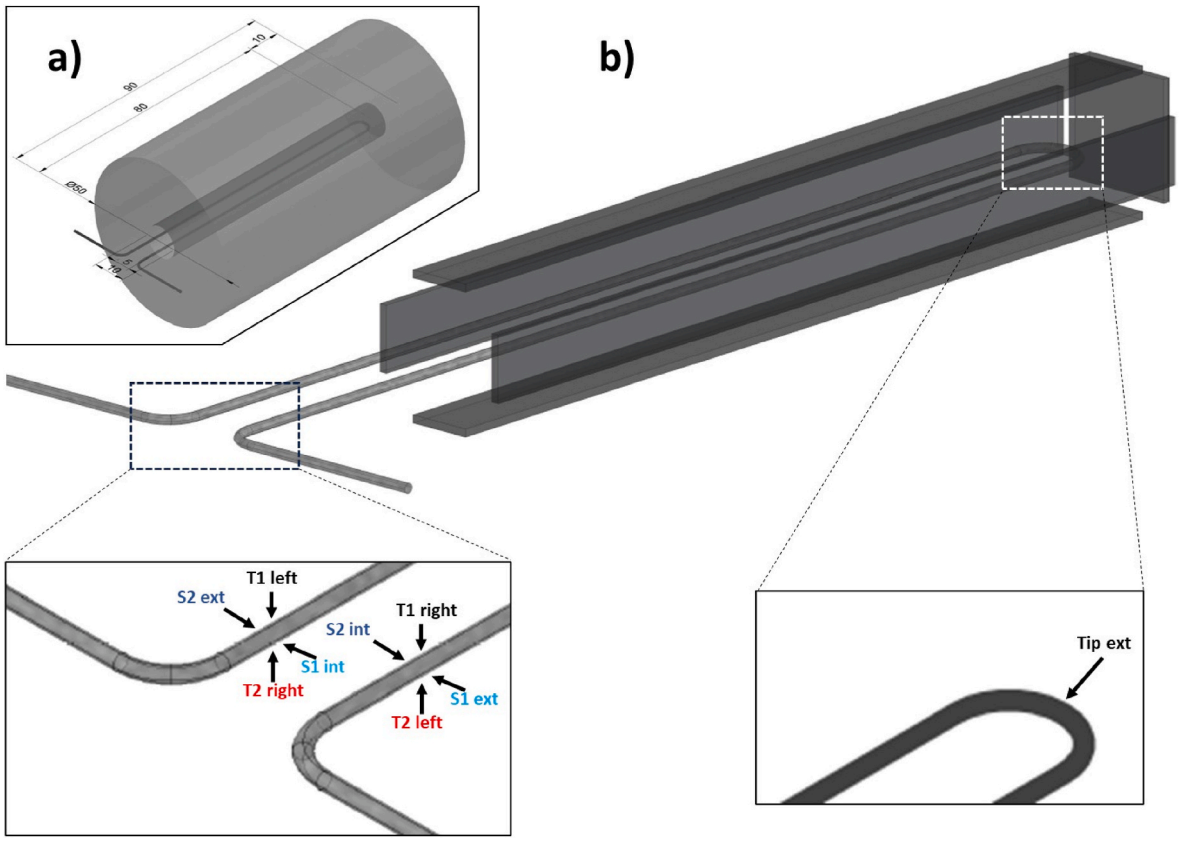

Fig. 1. a) Tungsten filament placed inside the hole of a coaxial germanium detector for the dopant evaporation; b) W filament surrounded by the five substrates, which mimic the walls of the hole of the Ge crystal. The substrates are placed in a purpose-built sample holder (see also Fig. 5). Insets: magnifications of the base (left) and tip (right) of the filament with the surfaces analysed by EDS highlighted (see text).

2.2. Film characterization

Scanning Electron Microscopy (SEM) was carried out using a microscope (Tescan Vega3 XM) equipped with the Energy Dispersive Spectrometry (EDS) option (EDAX). Rutherford Backscattering Spectrometry (RBS) was carried out using 2.0 MeV $^4He^+$ beam at the AN2000 Van de Graaff accelerator at the INFN Laboratori Nazionali di Legnaro with a 160° scattering angle.

The electrical activation of diffused Al and Sb was measured through the Van der Pauw-Hall technique, with a 4-point probe apparatus (4 PP). Spring loaded gold probes arranged in a square 4x4 mm^2 configuration suitable for our samples were placed on the corners of the laser spots, allowing ohmic contacts in all the measurements. Geometric correction factors were applied to the measurements to take into account for the finite size of the probes' tips, the difference between sample size and probes array size, the inhomogeneities in the doped layer and other deviations from ideality [19,20]. The instrument provides the doped layer sheet resistance RS and, with the application of a magnetic field (0.625T), the Hall coefficient RHS, from which the sheet Hall carrier density can be derived [21].

Secondary Ion Mass Spectrometry (SIMS) was performed on laser annealed samples, by using a Cameca IMS-4f instrument to characterize Al diffusion profiles. The profiles were acquired using a 5.5 keV Cs^+ primary beam and collecting $CsAl^+$ secondary ions. The depth scales have been calibrated assuming constant sputtering rate and measuring the crater depth using a stylus profilometer, with accuracy of ±2 %. Dopant concentrations were calibrated measuring reference samples of known areal densities with accuracies of ±10 %.

3. Results and discussion

3.1. Sputtering deposition on the filaments and their characterization by SEM-EDS and RBS

The first step in the process for the thin film deposition on the internal walls of a deep cavity involved sputtering deposition of the film containing the dopant element on W filaments. For p + doping, aluminum was deposited with germanium in a bilayer structure, according to the method described in Ref. [22]: Al layer was covered by Ge layer (cap layer). On the other hand, Sb was deposited alone for n + doping [23–25]. The filaments were previously cleaned with acetone and then heated until incandescence in high vacuum in order to remove any residual surface contaminants. Then they were fixed on the sample holder and inserted in the sputtering chamber. Two filaments were coated in each deposition run together with some substrates for subsequent analyses.

The choice of the thickness of the film to be sputter deposited on the wires has been done keeping in mind the elemental doses that must be deposited on the internal walls of the cavity. The latter ones were fixed starting from the results of previous work for Ge and Al (p + doping) [22] and for Sb (n + doping) [23–25]. Dose ranges for the three elements to achieve successful doping of germanium are reported in Table 1. These ranges are quite wide and allow for not too stringent requirements on the dose deposited on the filament.

Taking into account the very low pressure inside the evaporator and the very short distance between wire and walls, one can assume that all the evaporated atoms reach the walls by direct flight and condense there. If the W wire were single, infinitely long and positioned along the cavity axis and the film thickness were homogeneous on the whole wire, the evaporation would be isotropic and even the thickness of the

Table 1
Elemental doses of Al, Ge and Sb films: range of optimal doses for p+ and n + doping of Ge; range of doses to be deposited on the filament starting from formula (1); range of doses deposited on the filament and measured by EDS (Fig. 3); dose range expected on the walls after applying formula (1) to values in the previous column; range of doses deposited on the walls and measured by RBS (Fig. 6); dose in the laser annealed sample used for Van Der Pauw (VDP) measurements; dose of electrically active atoms in the laser annealed sample.

Element		Optimal dose range on the walls	Calculated dose range on the filament	Measured dose range on the filament	Expected dose range on the walls	Measured dose range on the walls	Dose in VDP sample	Electrically active dose	
	(atoms cm^{-2})								
Ge	Min	4.4e16	2.95e17	1.95e17	2.9e16	1.0e16	4.5e16	-	-
	Max	2.2e17	1.5e18	3.9e17	5.85e16	7.0e16		-	-
Al	Min	6.0e14	4.0e15	1.1e17	1.7e16	5.0e15	2.0e16	Min	4.0e15
	Max	2.4e16	1.6e17	2.3e17	3.45e16	3.5e16		Max	9.7e15
Sb[a]	Min	3.3e15	2.2e16	5.4e16	8.1e15	6.0e15	6.0e15	Min	2.0e15
	Max	2.6e16	1.75e17					Max	3.5e15

[a] For Sb, the dose was measured only in the central region of the filament on the T1 side and in the central region of T1 sample.

evaporated film would be homogeneous on all walls. In these conditions, the ratio between the elemental doses on the walls and those on the wire would be given by the inverse of the ratio between the respective surfaces per unit of wire length, e.g., in the case of Ge:

$$Ge_{wire}/Ge_{wall} = S_{wall}/S_{wire} \quad (1)$$

where Ge_{wire} and Ge_{wall} are Ge doses deposited on the wire and on the wall, respectively, S_{wire} and S_{wall} are the wire and wall surfaces per unit of wire length, respectively. In our setup the configuration necessarily presents the following differences (Fig. 1 a): i) there are two wires positioned off the axis so that their distance from the walls is not constant and one wire can also partially shade the other; ii) the wire length is finite; iii) the film thickness is not expected to be homogeneous on the whole wire. All these features lead to divergences from the above formula and to a dependence of the thickness from the position on the walls, both radial and longitudinal, which complicates the exact determination of the thickness in any position. In addition to this, the bottom of the cavity and the lateral walls close to it are in a very particular situation, with only one, curved wire in front of them. Keeping well in mind these considerations, as a first approximation we still chose to use formula (1) to determine the elemental amounts to be sputter deposited on the wires, after assuming as S_{wire} the total surface per unit of length of the two wires. This assumption leads to the dose ranges reported in Table 1.

After fixing the ranges of elemental doses, the next step is the measurement of the doses deposited on the wires. As a matter of fact, owing to the peculiar geometric characteristics of the wires, the doses cannot be simply inferred from previous calibration depositions on standard flat substrates, because the geometry of the latter is very different from that of the wires and the contribution coming from the deposition on shaded surfaces is absent. On the contrary, the direct measurement of deposited atoms on the wires would give the exact dose but unfortunately it cannot be accomplished using RBS technique for two main reasons: i) the wire surface is curved (not flat) and the wire diameter is smaller than the typical RBS spot size (1 mm); ii) the substrate is W, therefore the signals of the deposited elements overlap a very high background due to the substrate, which makes the acquisition time excessively long and the accuracy too low. The measurement technique chosen in this work to carry out this task was then Energy-Dispersive X-ray Spectrometry (EDS). Despite the inherent limitations of EDS, the intensity of the X-ray emission peaks of a specific element is related to the number of atoms of that element, in particular the higher the amount of a specific element in a film, the higher the number of normalized counts in its emission peak (peak integral). In order to evaluate the correlation between the peak integrals and the elemental doses, NIST DTSA-II software was used [26]. This software allows to simulate EDS measurements to achieve a quantitative analysis of the tested samples. In this context the analysis was limited to Ge and Al, but it can be applied to Sb as well. We simulated spectra of samples with the same Ge/Al atomic ratio but with different amounts of Ge and Al, after assuming the same experimental parameters (i.e., electron beam energy and current, acquisition time, etc.) for all the samples. Concerning beam energy, it has to be high enough for electrons to reach all deposited atoms, even the deepest ones, but it has also to be low enough to limit the probed volume to the film or a little more. The optimal energy can be either inferred from calculations of the mean free path of electrons in the sample (if the composition is known) or given, if the film is continuous on the entire surface of the sample, by the appearance of a substrate peak in the spectrum, which shows that some electrons pass through the entire film and reach the substrate. The integrals of the emission peaks of Ge and Al in the simulated spectra were calculated after background subtraction. Fig. 2 shows the peak integrals (calculated by the software for some prefixed Ge and Al doses) *vs* dose in a range going from $4x10^{16}$ to $8x10^{17}$ atoms cm^{-2} for Ge and from $2x10^{16}$ to $4x10^{17}$ atoms cm^{-2} for Al. For these measurements Ge and Al films deposited on C-coated Si substrates were used. As expected, the trend for both elements is not linear due to the self-absorption effect, which becomes more pronounced at increasing elemental dose and decreases the number of X-rays emitted from the sample and collected by the detector. However, this effect is not particularly evident in the range of our experimental data, which are also reported in the two graphs. The experimental integrals were calculated by the EDAX Genesis software after background subtraction. For experimental data as well as for simulations, the measurements were always carried out using the same parameters for all the samples. However, since NIST DTSA-II software cannot simulate the exact experimental setup used for these measurements (in particular, the EDS detector), experimental peak integrals were multiplied for the same scaling factor before inserting them into the graph in Fig. 2. This factor was calculated by dividing the simulated integral by the experimental integral of a sample in the central region of the dose range for both elements. A good agreement is observed, within the experimental error, between simulated and experimental data, indicating that EDS can be used to determine Ge and Al amounts on the wire.

Fig. 3 shows the results of the EDS measurements of Ge and Al amounts sputter-deposited on a W filament *vs* the distance from the filament tip: the relative normalized peak integrals (left axis) correspond to the elemental doses (right axis). Measurements were taken in different points of both branches of the filament (see Fig. 1). As can be seen, all data falls in a range between the maximum value ($3.9x10^{17}$ atoms cm^{-2} for Ge and $2.3x10^{17}$ atoms cm^{-2} for Al) and 50 % of it for both elements (see also Table 1). Considering the two sides of the filament facing the sputtering targets during the depositions (T1 and T2), about 10 % difference can be observed in the measured values of both elements for the two sides. This finding can be mainly ascribed to a small difference in the distance between filament and sputtering targets in the two depositions due to a not perfectly vertical position of the former: at these distances, a difference of 1 cm is sufficient to produce a 10 % variation in deposition rate. For both sides the trend of the elemental doses as a function of the position on the filament is directly related to the

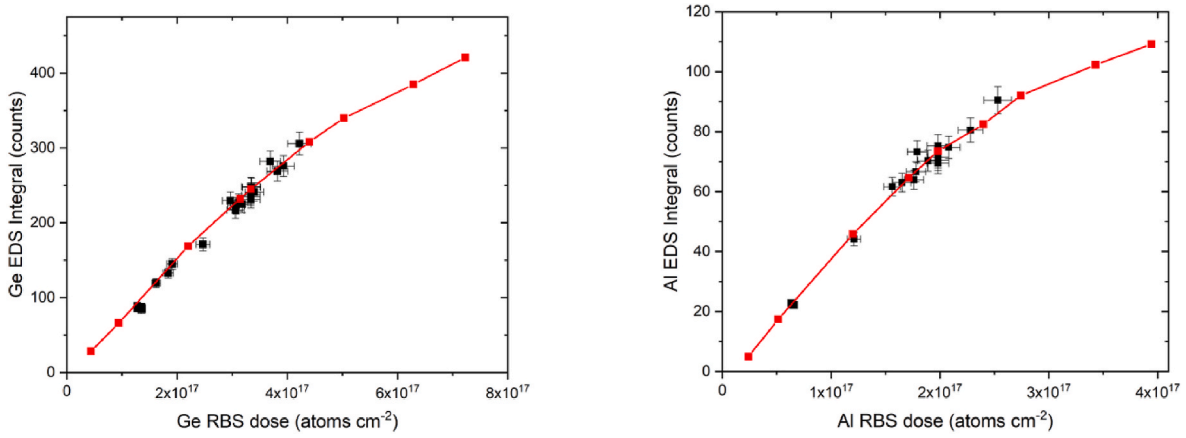

Fig. 2. Comparison between the integrals of the EDS theoretical peaks obtained by the NIST DTSA-II software (red points) and those of the experimental peaks measured by EDS and RBS (black points) on films deposited on C-coated Si substrates. The lines connect contiguous points.

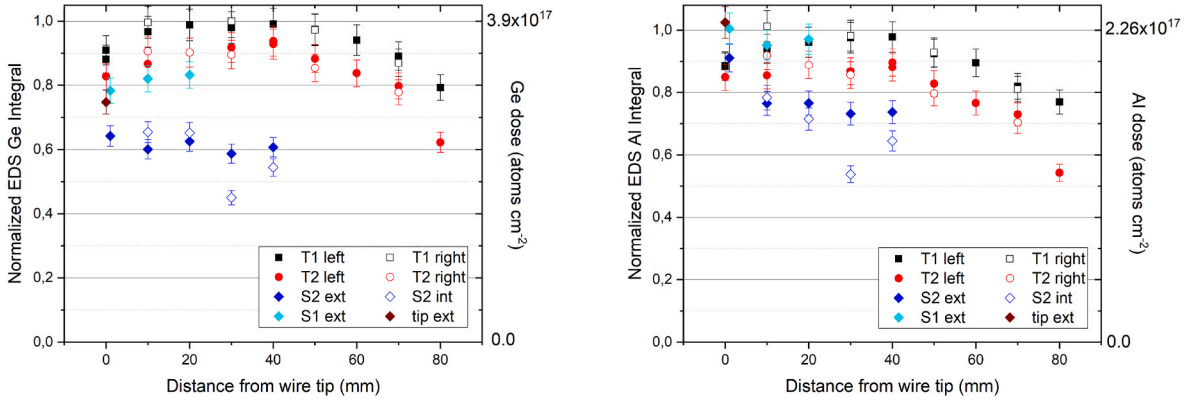

Fig. 3. Normalized EDS integral measured in different points on the W wire: Ge amount (left); Al amount (right). Every set of data refers to a specific surface on the wire (see Fig. 1) and the corresponding colour is the same used in Fig. 1.

deposition geometry: a region of homogeneous thickness (better than ±5 %) is centred about 30 mm from the tip and extends more than 40 mm. This trend reflects that expected in the case of depositions on flat substrates. Afterwards at increasing distances from the tip, the value clearly decreases. If we consider the lateral surfaces of the filament (S1 and S2), which were not completely in sight of both targets, the difference in quantity with respect to the surfaces T1 and T2 is not so marked: it is at most 40 % lower in the case of germanium and 30 % for aluminum. This difference appears to be related to the orientation of the surfaces: blue points, which correspond to surfaces placed to the left of T1, are lower than black and red points, especially for Ge, while cyan points (surface on the right of T1) are comparable to black and red points, particularly for Al. The reason of this correlation with orientation is not completely understood at the moment. On the other hand, the comparison between Ge and Al on these surfaces (S1 and S2) points out the higher value for Al regardless of orientation: this could be ascribed to a greater contribution of the diffuse component of the sputtered Al atoms than that of the Ge atoms. Comparing these values with dose ranges calculated from formula (1) and reported in Table 1, one can see that the measured Ge dose range is centred around the minimum of the corresponding calculated interval, while for Al the range is centred around the maximum. The expected dose ranges on the walls, calculated by applying formula (1) to the doses measured on the filament, are also reported in Table 1.

3.2. Calculation of the heating of the walls of the hole

Fig. 1 shows that the distance between the filament and the walls is only few mm. Since the filament is heated up to high temperatures (>1000 °C), the irradiated thermal power shall be taken into account, because all the thermal radiation hits the walls and the floor of the hole and it is well known that excessive heating irreparably compromises hyperpurity of germanium crystals. However, a simulation of the heating process shows that this effect can be neglected. Regarding the tungsten filament, it absorbs heat through Joule heating and gives it off through both irradiation to the inner Ge surface and thermal conduction to the metal clamps, which fix the ends of the filament. On the other hand, the inner walls of the hole absorb heat by irradiation and give it off through conduction in the Ge bulk to the outer surface.

From the energy conservation law for filament and Ge, one obtains the following system of two first order, non-linear, non-homogeneous equations:

$$\begin{cases} \dot{T_W} = \dfrac{V^2(t)}{C_W(T_W)\,R(T_W)} - \dfrac{S\,\varepsilon\,\sigma_{SB}}{C_W(T_W)}\left(T_W^4 - T_{Ge}^4\right) - \dfrac{k_W A_W}{C_W(T_W)\,L_W}\left(T_W - T_R\right) \\ \dot{T_{Ge}} = \dfrac{S\,\varepsilon\,\sigma_{SB}}{C_{Ge}(T_{Ge})}\,\dfrac{r_{Ge}}{2r_W}\left(T_W^4 - T_{Ge}^4\right) - \dfrac{k_{Ge} A_{Ge}}{C_{Ge}(T_{Ge})\,L_{Ge}}\left(T_{Ge} - T_R\right) \end{cases} \quad (2)$$

where subscripts W and Ge are referred to tungsten and germanium, respectively, T is the temperature, V the voltage across the filament, C the thermal capacity, R the filament resistance, S = 1.83 cm^{-2} the filament irradiating surface, $\varepsilon = 0.4$ the tungsten emissivity, σ_{SB} the Stefan-Boltzmann constant, k the thermal conductivity (k_W = 1.64 W cm^{-1} K^{-1},

$k_{Ge} = 0.58$ W cm^{-1} K^{-1}), A and L are the section and diffusion length for the Fourier law, respectively ($A_W = 0.001$ cm^2, $L_W = 1$ cm, $A_{Ge} = 0.245$ cm^2, $L_{Ge} = 2$ cm), r_{Ge} is the hole radius, r_W the filament radius, and T_R is the room temperature (300 K).

Taking into account that the wavelength of the radiation emitted from the W filament is peaked around 1 μm, the thickness of the Ge layer, which directly absorbs this radiation, is around 0.1 μm [27]. Therefore, in the calculations the inner surface of germanium has been treated as a 0.1-μm-thick cylindrical layer.

Temperature dependence of resistance, R, and thermal capacities, C_W and C_{Ge}, is given by the following equations:

$$\begin{cases} R(T_W) = R_0\left(1 + \alpha\, T_W + \beta\, T_W^2\right) \\ C_W(T_W) = \sum_{i=-1}^{3} a_i T_W^i \\ C_{Ge}(T_{Ge}) = C_{Ge} \end{cases} \quad (3)$$

where R is expanded to the second order term [28], C_W is taken from Ref. [29] and $C_{Ge} = 5\text{x}10^{-5}$ J K^{-1} is assumed to be constant.

The voltage and current measured during a typical filament heating run for the evaporation are shown in Fig. 4 a and b: after a first increase, the voltage is held constant to condition the filament and to stabilize the current, then it is rapidly increased to the maximum value, held for 3 s and then rapidly reduced to zero.

The experimental voltage values are used to create a voltage profile for the simulation. After fixing the starting point with both unknown temperatures at 300K, we evaluated tungsten resistance and thermal capacities at room temperature from equation (2). By substituting these values into the rightmost side of the system of equation (1) and multiplying both equations for a time step small enough to ensure convergence (100 μs), new temperatures were achieved. These steps were then repeated until the end of the process (50 s) thus obtaining the evolution of T_W and T_{Ge}. By substituting the T_W profile into the resistance formula, resistance trend over time was obtained and used together with the voltage profile to extrapolate a current profile (Fig. 4 b). This profile was then compared to the experimental values, measured with an amperometric clamp, to adjust some experimental parameters. The simulation

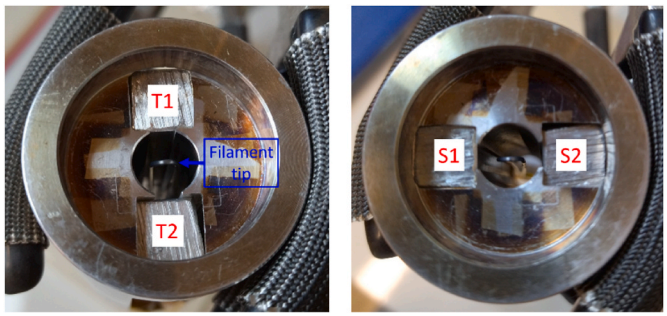

Fig. 5. Filament tip inside the dummy (view from the hole floor). Left: substrates are placed above and below the filament (T1 and T2, respectively). Right: substrates are placed on the sides of the filament (S1 and S2). The substrate positioned on the floor of the hole is not present.

was subsequently repeated with small changes of these parameters (in fact, the filament is treated as a thermally homogeneous object for simplicity, but it surely is not) until obtaining the best matching between the experimental profile and the simulated one. The closest current profiles were finally obtained from this numerical Euler solution and gave the evolution of the two temperatures (Fig. 4 c and d).

It is noteworthy that, while the filament temperature reaches a maximum value of about 1500 °C, the temperature increase of the internal walls of the hole is very limited (less than 25 °C). Therefore, the outcome of this calculation allows to exclude the excessive heating of germanium and the consequent incorporation of contaminating species.

3.3. Evaporation on substrates placed inside a purpose-built sample holder

The filament coated by the sputtered film was placed inside the vacuum evaporation chamber and inserted in a purpose-built sample holder (dummy), which mimics a HPGe coaxial crystal (Fig. 5). The substrates are placed on two rows along the entire length of the hole and on the floor of the hole facing the filament tip. In order to achieve a complete characterization of the evaporation on the hole walls, two evaporation runs were carried out with the substrates put in different

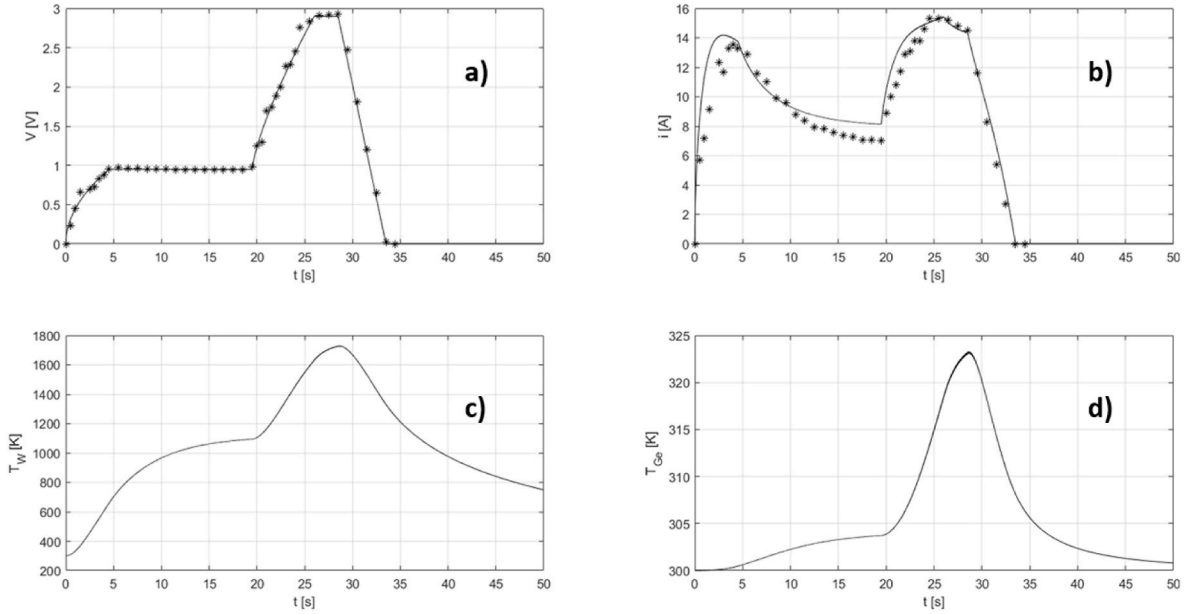

Fig. 4. a) Experimental values of the voltage across the filament (discrete points) and simulated voltage profile (solid line) as a function of time. AC voltage is represented as DC for clarity, but simulations were performed with AC voltage. b) Experimental values of the current through the filament (discrete points) and simulated current profile (solid line) as a function of time. c) Time evolution of filament temperature (T_W). d) Time evolution of the temperature of the internal walls of the hole (T_{Ge}).

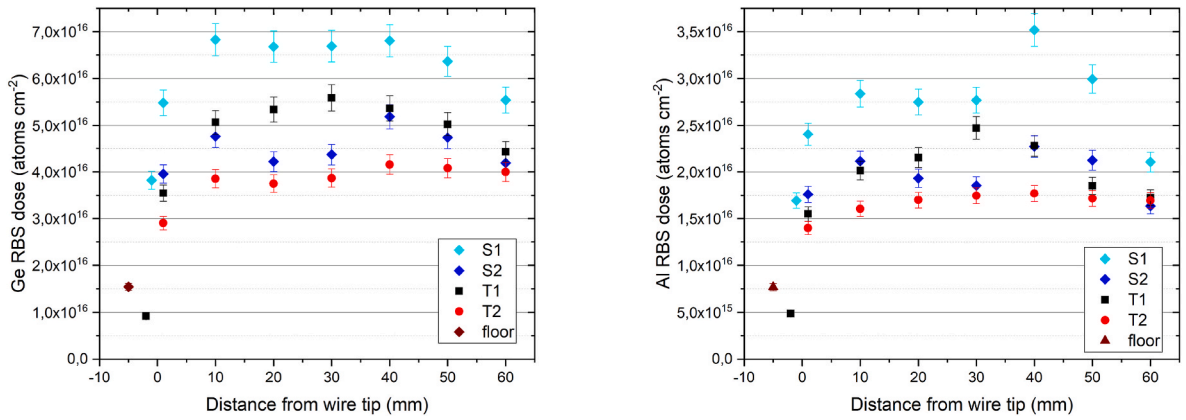

Fig. 6. RBS doses measured in different points of the substrates placed inside the hole during the evaporation: Ge (left) and Al (right). Data relative to distance of -5 mm (brown points) refer to the substrate placed on the hole floor.

positions with respect to the filament: in the first configuration, the substrates faced the surfaces T1 and T2 of the filament (Fig. 5); in the second one, the dummy was rotated 90° and the substrates faced the lateral surfaces (S1 and S2).

After positioning filament and substrates and evacuating the chamber down to a pressure lower than $2x10^{-5}$ Pa, the evaporation runs were carried out by increasing the current in the filament up to the maximum value of 15 A, keeping it constant for only 3 s and then rapidly decreasing it to zero. Throughout the process the pressure was always below $2x10^{-5}$ Pa. After the evaporation the filament was analysed by EDS and the lack of Ge and Al signals confirmed the successful evaporation of both elements.

Fig. 6 shows the Ge and Al doses deposited in the two configurations as measured by RBS. The presence of W in the evaporated films was also investigated and its amount was found to be less than $2x10^{13}$ atoms cm^{-2}.

Considering the trend of the doses with the distance from the tip, at fixed side (e.g., T1), we see that they are quite homogeneous in a central region from 10 to 50 mm (±10 % of the average value, except for side S1 of Al). This region (hereafter the central region) is important because all points within it face the same type of evaporation source (i.e., in this region a filament of infinite length could be assumed). This is not the case near the tip of the filament and, in particular, on the hole floor and indeed in these latter points the doses decrease significantly. A comparison of the doses at fixed distance in the central region shows that they follow this order on average: S1>T1>S2>T2. This trend can be partly explained if one considers the doses sputter-deposited on the filament, which are the corresponding evaporation sources (data in Fig. 3). In fact, due to the geometric configuration of the evaporation setup, each of the four substrates predominantly receives evaporated atoms from the sides of the filament they face. The large difference between S1 and S2 in Fig. 6 (S1>>S2) for both Ge and Al mirrors the difference between the corresponding doses sputtered on the filament (cyan and blue points in Fig. 3). The same relation is found also between T1 and T2 (T1>T2) although the difference is less pronounced. If one compares S1 and S2 with T1 and T2 for both Ge and Al in sputtered films (Fig. 3) and evaporated films (Fig. 6), one finds that the former are both increased with respect to the latter in the evaporated samples. This finding is ascribed to geometrical reasons: the solid angle subtended by the lateral surface is greater than that of the surface in front of the wires even if there are two wires. A comparison between measured and predicted dose ranges for both elements (Table 1) shows that they are not very different, especially if one neglects the points closest to the wire tip. Moreover, all the measured doses are very close to the optimal ones. From these results one can draw the following important indications to improve the homogeneity of deposition on the hole walls and floor: i) the elemental doses deposited on the T1 and T2 surfaces must be the same (T1 = T2 = T); ii) the elemental doses deposited on the S1 and S2 surfaces must be the same (S1═S2═S), but they have to be lower than those deposited on T1 and T2 (S < T); probably a quantity close to that of S2 would be right; iii) the doses deposited on the filament tip should be significantly increased. It is also particularly noteworthy that formula (1) gives a reasonably accurate estimate of the elemental dose deposited on the walls of the hole.

3.4. Laser annealing treatments and electrical activation measurements

For the electrical activation measurements Ge and Al were evaporated on Ge substrates and then laser annealed to promote Al diffusion and doping. Taking into account the results obtained in Ref. [22], the recipes used for the laser included a pre-annealing step (single pulse with 100 mJ cm^{-2} energy density) followed by up to 4 pulses with 500 mJ cm^{-2} energy density. SEM images of a $GeAl_x$ film evaporated on a Ge substrate, before and after laser annealing, are shown in Fig. 7: the featureless surface typical for a vacuum-deposited film evolves to a different morphology as a consequence of the laser treatment.

Fig. 8 shows the SIMS measurements of a sample after laser annealing with 1 pulse and 4 pulses, respectively. The depth scale was calibrated measuring the crater depths with a stylus profilometer and assuming constant sputtering rate, while the chemical concentration calibration was performed using a suitable standard. Fig. 8 clearly shows that in both cases, as a result of the PLM processes, Al has diffused into the Ge bulk. Increasing the number of laser pulses, i.e. increasing the number of diffusion steps, the incorporated dopant is redistributed more deeply in the molten layer, while decreasing the surface concentration, which is still higher than 10^{20} cm^{-3} in both cases. No clear signs of surface segregation, neither out-diffusion are present.

The electrical activation of Al atoms diffused in the annealed samples was also measured by the Van der Pauw-Hall technique, using a 4-point probe apparatus. Samples annealed with 4 pulses show a successful activation of positive carriers with a dose ranging from $4x10^{15}$ to $9.7x10^{15}$ cm^{-2} (Table 1) and a sheet resistance between 65 and 88 Ω/sq. Considering that the total Al dose in these evaporated films is around $2x10^{16}$ atoms cm^{-2} (S2 samples), the percentage of electrically active atoms ranges from 20 % to 48 %. This range of values is slightly lower than that obtained with Al films directly sputtered on germanium (from 30 % to 100 % [22]). On the other hand, in the samples annealed with either 1 pulse or 2 pulses the dose of active carriers is too low to be measured and they result inactive.

After this successful result with p-type doping, we applied the same method to obtain n-type doping of germanium using antimony. Sb film was deposited by sputtering on the filament and its average dose as measured by EDS was $5.4x10^{16}$ atoms cm^{-2} (Table 1). Since Sb doping is not particularly affected by oxygen incorporation, no special

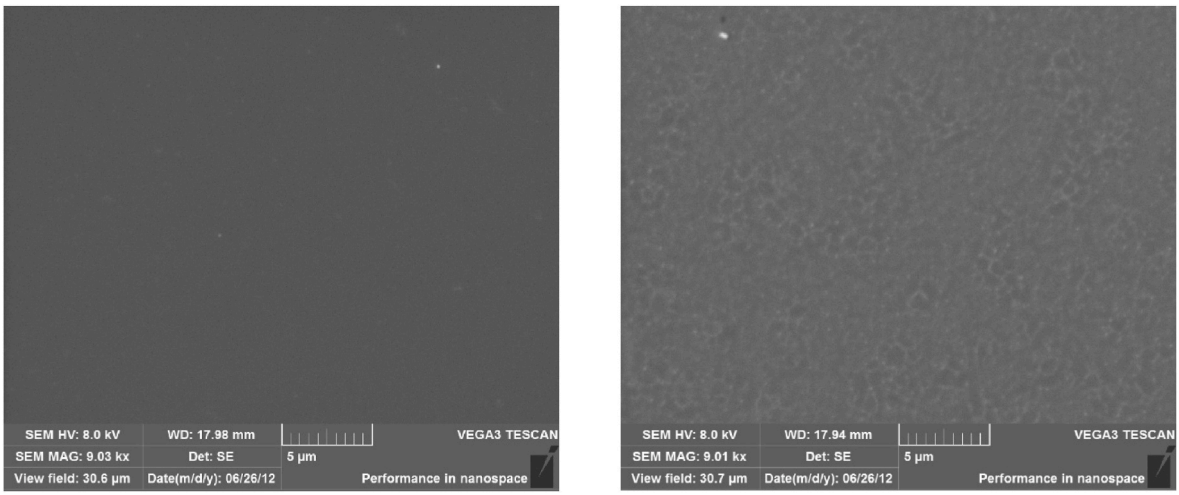

Fig. 7. SEM images of a Ge sample with a $GeAl_x$ evaporated film: as deposited (left) and after laser annealing with 4 pulses (right).

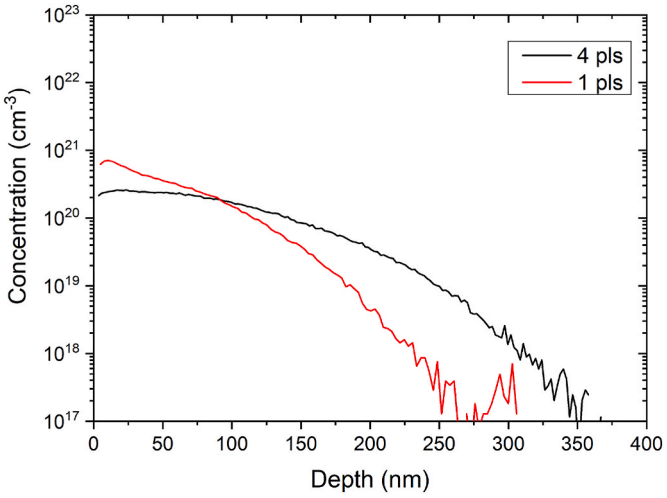

Fig. 8. SIMS chemical concentration profiles of Al diffused in germanium after laser annealing with 1 pulse (red line) and 4 pulses (black line).

precautions were taken. Sb evaporation from the filament was carried out at a pressure lower than $2x10^{-3}$ Pa. The average Sb dose as measured by RBS in the evaporated film in the central region was $6.0x10^{15}$ atoms cm^{-2}. The films evaporated on Ge substrates were annealed with either 1, 4 or 8 laser pulses with 500 mJ cm^{-2} energy density per pulse. SEM images of these samples (not shown) pointed out that the featureless surface of the as-deposited films was maintained even after the laser treatment. Unlike aluminum-containing samples, all antimony-doped samples exhibited a significant dose of active carriers regardless of the laser treatment undergone: at increasing number of pulses, the sheet resistance decreased from 15 to 8 Ω/sq, while the dose of active carriers increased from $2.0x10^{15}$ to $3.5x10^{15}$ cm^{-2} (Table 1). It is noteworthy that the percentage of electrically active Sb atoms in the evaporated films is comparable to that in the films sputtered directly on the Ge substrates and subjected to the same laser treatments: as a matter of fact, it ranges from 33 % (1 pls) to 58 % (8 pls) in the former and from 40 % (1 pls) to 56 % (8 pls) in the latter [24,30]. Considering that the activation rate of Sb obtained with equilibrium doping processes is usually modest compared to other dopant elements such as Al [31,32], the high dose of active atoms obtained for these samples is a confirmation of the effectiveness of PLM as a Ge doping technique [10,24].

4. Conclusions

This work describes a relatively simple method for the deposition of thin films on the inner walls of a deep blind hole with a 10 mm diameter and an aspect ratio up to 8:1. The method consists in the film evaporation from a tungsten filament suitably coated by the selected metal and in its deposition on the walls of the hole. To test the method, a co-deposition of Ge and Al and a deposition of Sb have been carried out. The first step of the process is the sputter deposition of the source film ($GeAl_x$ or Sb) on the W filament and the characterization of the film thickness and homogeneity. The thickness of the source film has been chosen taking into account the thickness of the film on the walls of the hole and the evaporation geometry. It has been found that the thickness is well correlated to that of the evaporated film and the correlation is essentially of a geometric nature. A uniform thickness distribution on the walls of the hole can be obtained with a suitable choice of the thickness distribution of the film deposited on the wire. Owing to the peculiar properties of the tungsten filament as a substrate (small diameter and high atomic weight) the measurement of the thickness has been done by EDS technique, after a calibration by means of RBS measurements of selected samples. As a second step, the filament has been placed inside the hole and heated by passing current through it until the complete evaporation of the sputtered film. The evaporations have been done inside a dummy suitably made to simulate a HPGe crystal. In spite of the high temperature reached by the filament (around 1500 °C), a theoretical calculation showed that the increase of temperature of the inner walls of the hole during filament heating is only a few tens of degrees. This finding guarantees the compatibility of this method with the application for which it was developed, i.e., doping of hyperpure germanium crystals to be used in gamma radiation detectors. The limited increase of temperature allows to preserve the Ge hyperpurity and to exclude the incorporation of contaminants in the HPGe crystal.

Films of $GeAl_x$ and Sb were evaporated on germanium substrates suitably placed inside the dummy to mimic the walls of the hole and were undergoing pulsed laser melting treatment to obtain the doping of germanium surface. For both materials the van der Pauw measurements revealed the electrical activation of a significant fraction of doped atoms, thus confirming that this technique can be used for both p+ and n + doping of the internal walls of a hole in a hyperpure germanium crystal for the detection of gamma rays.

Declaration of competing interest

The authors declare that they have no known competing financial interests or personal relationships that could have appeared to influence

the work reported in this paper.

Data availability

Data will be made available on request.

Acknowledgements

Massimo Loriggiola (LNL-INFN) is acknowledged for their precious technical assistance.

References

[1] R. Wei, C. Rincon, T.L. Booker, J.H. Arps, 188–189, Surf. Coat. Technol. (2004) 691.
[2] W. Ensinger, Rev. Sci. Instrum. 67 (1) (1996) 318.
[3] M. Yang, A.A.I. Aarnink, J. Schmitz, A.Y. Kovalgin, Thin Solid Films 646 (2018) 199.
[4] M. Knaut, M. Junige, V. Meumann, H. Wojcik, T. Henke, C. Hossbach, A. Hiess, M. Albert, J.W. Bartha, Microelectron. Eng. 107 (2013) 80.
[5] C.-G.- Kim, W.-J. Lee, Thin Solid Films 519 (2010) 74.
[6] J. Eberth, H. Hess, P. Reiter, S. Bertoldo, C. Carraro, G. Maggioni, D.R. Napoli, W. Raniero, D. De Salvador, Agata detector technology: recent progress and future developments, Eur. Phys. J. A 59 (2023) 179.
[7] G.S. King III, F.T. Avignone III, C.E. Cox, T.W. Hossbach, W. Jennings, J.H. Reeves, Nucl. Instrum. Methods Phys. Res. 595 (2008) 599.
[8] V. Boldrini, G. Maggioni, S. Carturan, W. Raniero, F. Sgarbossa, R. Milazzo, D. R. Napoli, E. Napolitani, R. Camattari, D. De Salvador, J. Phys. D Appl. Phys. 52 (2019) 035104.
[9] F. Sgarbossa, Mater. Sci. Semicond. Process. 167 (2023) 107795.
[10] F. Sgarbossa, G. Maggioni, G.A. Rizzi, S.M. Carturan, E. Napolitani, W. Raniero, C. Carraro, F. Bondino, I. Píš, D. De Salvador, Appl. Surf. Sci. 496 (2019) 143713.
[11] G. Maggioni, F. Sgarbossa, E. Napolitani, W. Raniero, V. Boldrini, S.M. Carturan, D. R. Napoli, D. De Salvador, Mater. Sci. Semicond. Process. 75 (November 2017) (2018) 118–123.
[12] F. Sgarbossa, S.M. Carturan, D. De Salvador, G.A. Rizzi, E. Napolitani, G. Maggioni, W. Raniero, D.R. Napoli, G. Granozzi, A. Carnera, Nanotechnology 29 (2018), 465702.
[13] F. Sgarbossa, A. Levarato, S.M. Carturan, G.A. Rizzi, C. Tubaro, G. Ciatto, F. Bondino, I. Píš, E. Napolitani, D. De Salvador, Appl. Surf. Sci. 541 (2021) 148532.
[14] L.I. Maissel and R. Glang, Handbook of Thin Film Technology, 1983 Reissue, McGraw-Hill Inc., p. 1-39.
[15] P.N. Luke, IEEE trans. Nucl. Sci. NS-31 (1984) 312.
[16] A.P. Bradford, G. Hass, J.F. Osantowski, A.R. Toft, Appl. Opt. 8 (1969) 1183.
[17] Q. Looker, Fabrication Process Development for High-Purity Germanium Radiation Detectors with Amorphous Semiconductor Contacts, PhD Thesis, University of California, Berkeley, 2014.
[18] R. Milazzo, M. Linser, G. Impellizzeri, D. Scarpa, M. Giarola, A. Sanson, G. Mariotto, A. Andrighetto, A. Carnera, E. Napolitani, Appl. Surf. Sci. 509 (2020) 145230.
[19] J.D. Weiss, Solid State Electron. 62 (2011) 123.
[20] O. Bierwagen, T. Ive, C.G. Van de Walle, J.S. Speck, Appl. Phys. Lett. 93 (2008) 242108.
[21] B. Onsia, T. Conard, S. De Gendt, M.M. Heyns, I. Hoflijk, P.W. Mertens, M. Meuris, G. Raskin, S. Sioncke, I. Teerlinck, A. Theuwis, J. Van Steenbergen, C. Vinckier, Solid State Phenom. 103–104 (2005) 27.
[22] G. Maggioni, D. De Salvador, D.R. Napoli, E. Napolitani, p+ or n+ type doping process for semiconductors, International Patent WO 2021/214028 A1 (October 2021) 28.
[23] G. Maggioni, S. Carturan, W. Raniero, S. Riccetto, F. Sgarbossa, V. Boldrini, R. Milazzo, D.R. Napoli, D. Scarpa, A. Andrighetto, E. Napolitani, D. De Salvador, Eur. Phys. J. A 54 (2018) 34.
[24] C. Carraro, R. Milazzo, F. Sgarbossa, D. Fontana, G. Maggioni, W. Raniero, D. Scarpa, L. Baldassarre, M. Ortolani, A. Andrighetto, D.R. Napoli, D. De Salvador, E. Napolitani, Appl. Surf. Sci. 509 (2020) 145229.
[25] S. Bertoldo, G. Maggioni, W. Raniero, C. Carraro, S. Riccetto, F. Sgarbossa, D. Scarpa, A. Andrighetto, A. Mazzolari, A. Gadea, D.R. Napoli, E. Napolitani, D. De Salvador, Eur. Phys. J. A 57 (2021) 177.
[26] https://www.nist.gov/services-resources/software/nist-dtsa-ii. (Accessed 10 November 2023).
[27] H.P. Philipp, E.A. Taft, Phys. Rev. 113 (4) (1959) 1002.
[28] D. Lide, CRC Handbook of Chemistry and Physics, 75 edition, CRC Press, 1995, p. 12.
[29] G.K. White, S.J. Collocott, Heat capacity of reference materials: Cu and W, J. Phys. Chem. Ref. Data 13 (4) (1984) 1251.
[30] C. Carraro, Hyperdoping of Germanium by pulsed laser melting. PhD Thesis, University of Padua, Padua, Italy, 2021.
[31] R. Duffy, E. Napolitani, F. Cristiano, Chapter 5 - *Materials science issues related to the fabrication of highly doped junctions by laser annealing of Group IV semiconductors*, Editor(s): Fuccio Cristiano, Antonino La Magna, in: Woodhead Publishing Series in Electronic and Optical Materials, Laser Annealing Processes in Semiconductor Technology, 2021, pp. 175–250, https://doi.org/10.1016/B978-0-12-820255-5.00007-6. Woodhead Publishing.
[32] K. Nozawa, T. Nishida, T. Ishiyama, T. Suemasu, K. Toko, n-Type polycrystalline germanium layers formed by impurity-doped solid-phase growth, ACS Appl. Electron. Mater. 5 (2023) 1444–1450, https://doi.org/10.1021/acsaelm.2c01381.